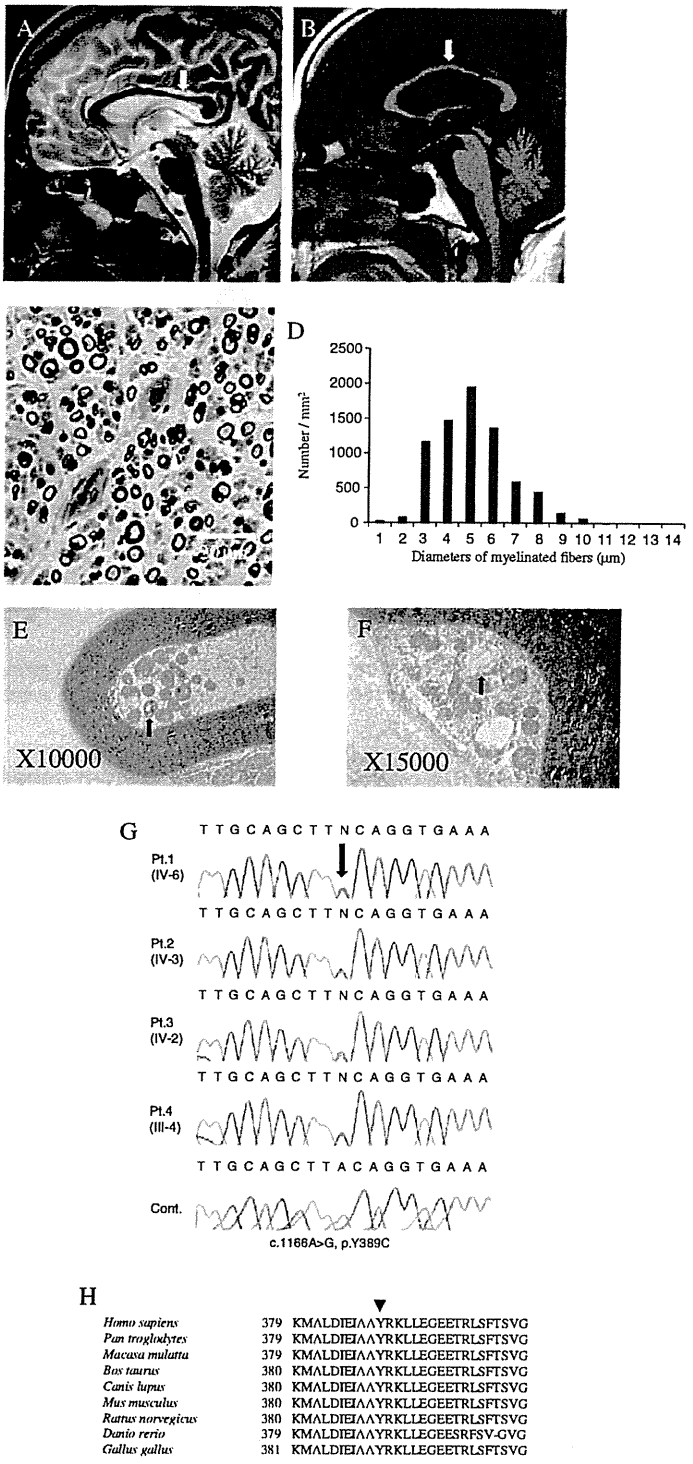


**Figure 2.** Radiological, pathological and genetic findings of the hereditary motor and sensory neuropathy-V (HMSN-V) family. (A) Brain magnetic resonance imaging (MRI) of patient 1 and (B) patient 2 showing a thin corpus callosum (arrows). (C) Toluidine blue and safranin staining of left sural nerve from patient 2 shows occasional small fiber clusters (arrowheads). (D) Histogram of myelinated fibers. (E, F) Electron microscope images show mitochondrial accumulation and abnormal mitochondrial structure (arrow) in neuron (E) and Schwann cell (F). (G) Chromatogram of the heterozygous c.1166A>G (Y389C) mutation in exon 2 of NEFL: upper, four affected members; bottom, control. (H) Comparison of aligned NEFL amino acid sequences between species. Arrow head (▼) indicates the mutated amino acid.

**Table 1.** Nerve conduction studies in patients 1 and 2.

| | Median | | | | Ulnar | | | | Tibial | | Peroneal | | Sural | |
|---|---|---|---|---|---|---|---|---|---|---|---|---|---|---|
| Nerve | MCV (>49.6) | CMAP (>3.1) | SCV (>47.2) | SNAP (>7.0) | MCV (>50.1) | CMAP (>6.0) | SCV (>46.9) | SNAP (>6.9) | MCV (>41.7) | CMAP (>4.4) | MCV (>41.8) | CMAP (>6.7) | SCV (>40.8) | SNAP (>5.0) |
| Pt. 1 | 48.7 | 9.2 | N.R. | N.R. | 50 | 8.8 | N.R. | N.R. | 33.3 | 4.1 | 36.4 | 2.9 | N.R. | N.R. |
| Pt. 2 | 48.2 | 7.5 | 41.6 | 7.4 | 52.3 | 3.8 | N.R. | N.R. | 38.8 | 2 | 32.1 | 0.2 | N.R. | N.R. |

CMAP, compound muscle action potential; MCV, motor conduction velocity; N.R., not recordable; Pt, patient; SCV, sensory conduction velocity; SNAP, sensory nerve action potential.

## Discussion

All four patients showed a gradually progressing spastic gait, which along with findings from physical examinations and nerve conductions, confirmed the involvement of upper motor neurons and sensory and motor peripheral nerves. MRI of patients 1 and 2 revealed unremarkable changes other than a markedly thin corpus callosum, a structural abnormality not previously reported in patients with NEFL mutations, but common in some forms of SPG. To the best of our knowledge, no pyramidal tract disorder has been noted in any patients with NEFL mutations.

*NEFL* encodes the neurofilament light polypeptide (NF-L), the smallest of the three neurofilament isoforms, and a cytoskeletal protein almost universally expressed in the central nervous system (CNS), and peripheral nervous system (PNS). At the subcellular level, neurofilaments are observed in the somata, axons, and dendrites, where they control developmental and plastic changes in the neuronal morphology.

NF-L is divided into the following three domains: head, rod, and tail. Several mutations that cause CMT type 1F or 2E are distributed in the head or rod domain, whereas the p.Y389C mutation is located in the Coil2B section of the rod domain. The following three additional mutations in the Coil2B domain were reported in patients with CMT: p.Q333P, p.L334P, and p.E397K *(Mersiyanova et al., 2000; Choi et al., 2004)*. Including these, all NEFL mutations, autosomal dominant p.P8R, p.P8Q, p.P8L, p.T21fs, p.P22T, p.P22S, p.E89K, p.L93P, p.N97S, p.A148V, p.Q333P, p.L334P, E397K, and autosomal recessive p.E210X, do not cause pyramidal signs *(Mersiyanova et al., 2000; De Jonghe et al., 2001; Georgiou et al., 2002; Yoshihara et al., 2002; Jordanova et al., 2003; Choi et al., 2004; Leung et al., 2006; Miltenberger-Miltenyi et al., 2007; Yum et al., 2009)*. However, some patients with autosomal dominant p.L93P mutation had cerebellar ataxia and schizophrenia *(Miltenberger-Miltenyi et al., 2007)*, and a patient with autosomal dominant p.N97S mutation had learning disorder and nystagmus *(Jordanova et al., 2003)*. Furthermore some patients with autosomal recessive p.E210X mutation had learning disorder and prolonged visual-evoked responses *(Yum et al., 2009)*. These findings suggest the potential to cause CNS disorders by *NEFL* mutation.

Another NF-L mutation altered the intracellular distribution of mitochondria in cultured neurons *(Perez-Olle et al., 2004)*. Mutations in *MFN2*, a gene associated with both CMT and HMSN with pyramidal signs, may cause axonal damage by mitochondrial fusion disorder. Similarly, the abnormal mitochondria and mitochondrial accumulation in the neurons and Schwann cells in our patient, NEFL mutation may also result in axonal damage by altered mitochondrial distribution both in PNS and CNS because of the broad pattern of expression.

## Acknowledgements

We thank the family members described in this report for their cooperation. We also thank Y. Mori and A. Nishibeppu of Kagoshima University for excellent technical assistance. This study was supported in part by grants from the Nervous and Mental Disorders and Research Committee for Charcot-Marie-Tooth Disease, Neuropathy, Ataxic Disease and Applying Health and Technology of the Japanese Ministry of Health, Welfare and Labour (H. T.). The authors would like to thank Enago (www.enago.jp) for the English language review.

## References

Borhoumi C, Amouri R, Ben Hamida C, Ben Hamida M, Machghoul S, Gueddiche M, Hentati F (2001). Linkage of a new locus for autosomal recessive axonal form of Charcot-Marie-Tooth disease to chromosome 8q21.3. Neuromuscul Disord 11:27–34.

Choi BO, Lee MS, Shin SH, Hwang JH, Choi KG, Kim WK, Sunwoo NI, Kim NK, Chung KW (2004). Mutational analysis of PMP22, MPZ, GJB1, EGR2 and NEFL in Korean Charcot-Marie-Tooth neuropathy patients. Hum Mutat 24:185–186.

De Jonghe P, Mersivanova I, Nelis E, Del Favero J, Martin JJ, Van Broeckhoven C, Evgrafov O, Timmerman V (2001). Further evidence that neurofilament light chain gene mutations can cause Charcot-Marie-Tooth disease type 2E. Ann Neurol 49:245–249.

Georgiou DM, Zidar J, Korosec M, Middleton LT, Kyriakides T, Christodoulou K (2002). A novel NF-L mutation Pro22Ser is associated with CMT2 in a large Slovenian family. Neurogenetics 4:93–96.

Goto H, Matsuo H, Ohnishi A, Fukudome T, Shibuya N (2003). X-linked motor and sensory neuropathy with pyramidal signs and cerebral white matter lesions. Muscle Nerve 28:623–625.

Irobi J, Van den Bergh P, Merlini L, Verellen C, Van Maldergem L, Dierick I, Verpoorten N, Jordanova A, Windpassinger C, De Vriendt E, Van Gerwen V, Auer-Grumbach M, Wanger K, Timmerman V, De Jonghe P (2004). The phenotype of motor neuropathies associated with BSCL2 mutations is broader than Silver syndrome and distal HMN type V. Brain 127:2124–2130.

Jordanova A, De Jonghe P, Boerkoel CF, Takashima H, De Vriendt E, Ceuterick C, Martin JJ, Butler IJ, Mancias P, Papasozomenos SC, Terespolsky D, Potocki L, Brown CW, Shy M, Rita DA, Tournev I, Kremensky I, Lupski JR, Timmerman V (2003). Mutations in the neurofilament light chain gene (NEFL) cause early onset severe Charcot–Marie–Tooth disease. Brain 126:590–597.

Klebe S, Azzedine H, Durr A, Bastien P, Bouslam N, Elleuch N, Forlani S, Charon C, Koenig M, Melki J, Brice A, Stevanin G (2006). Autosomal recessive spastic paraplegia (SPG30) with mild ataxia and sensory neuropathy maps to chromosome 2q37.3. Brain 129:1456–1462.

Leung CL, Nagan N, Graham TH, Liem RKH (2006). A novel duplication/insertion mutation of NEFL in a patient with Charcot-Marie-Tooth disease. Am J Med Genet A 140:1021–1025.

Luigetti M, Fabrizi GM, Madia F, Ferrarini M, Conte A, Delgrande A, Tonali PA, Sabatelli M (2010). Seipin S90L mutation in an Italian family with CMT2/dHMN and pyramidal signs. Muscle Nerve 42:448–451.

Mersiyanova IV, Perepelov AV, Polyakov AV, Sitnikov VF, Dadali EL, Oparin RB, Petrin AN, Evgrafov OV (2000). A new variant of Charcot-Marie-Tooth disease type 2 is probably the result of a mutation in the neurofilament-light gene. Am J Hum Genet 67:37–46.

Miltenberger-Miltenyi G, Janecke AR, Wanschitz JV, Timmerman V, Windpassinger C, Auer-Grumback M, Loscher WN (2007). Clinical and electrophysiological features in Charcot-Marie-Tooth disease with mutations in the NEFL gene. Arch Neurol 64:966–970.

Murphy SM, Herrmann DN, McDermott MP, Scherer SS, Shy ME, Reilly MM, Pareyson D (2011). Reliability of the CMT neuropathy score (second version) in Charcot-Marie-Tooth disease. J Peripher Nerv Syst 16:191–198.

Okamoto K, Ito J, Tokiguchi S (1990). The MR findings of the corpus callosum of normal young volunteers. Nihon Igaku Hoshasen Gakkai Zasshi 50:954–963.

Patel H, Cross H, Proukakis C, Hershberger R, Bork P, Ciccarelli FD, Patton MA, McKusick VA, Crosby AH (2002). SPG20 is mutated in Troyer syndrome: an hereditary spastic paraplegia. Nat Genet 31:347–348.

Perez-Olle R, Jones ST, Liem RK (2004). Phenotypic analysis of neurofilament light gene mutations linked to Charcot-Marie-Tooth disease in cell culture models. Hum Mol Genet 13:2207–2220.

Rainier S, Bui M, Mark E, Thomas D, Tokarz D, Ming L, Delaney C, Richardson RJ, Albers JW, Matsunami N, Stevens J, Coon H, Leppert M, Fink JK (2008). Neuropathy target esterase gene mutations cause motor neuron disease. Am J Hum Genet 82:780–785.

Windpassinger C, Auer-Grumbach M, Irobi J, Patel H, Patek E, Höri G, Malli R, Reed JA, Dierick I, Verpoorten N, Warner TT, Proukakis C, Van den Bergh P, Varellen C, Van Maldergem L, Merlini L, De Jonghe P, Timmerman V, Crosby AH, Wagner K (2004). Heterozygous missense mutations in BSCL2 are associated with distal hereditary motor neuropathy and Silver syndrome. Nat Genet 36:271–276.

Yoshihara T, Yamamoto M, Hattori N, Misu K, Koike H, Sobue G (2002). Identification of novel sequence variants in the neurofilament-light gene in a Japanese population: analysis of Charcot-Marie-Tooth disease patients and normal individuals. J Peripher Nerv Syst 7:221–224.

Yum SW, J-x Z, Mo K, Li J, Scherer SS (2009). A novel recessive NEFL mutation causes a severe, early-onset axonal neuropathy. Ann Neurol 66:759–770.

Zhao Z, Hashiguchi A, Hu J, Sakiyama Y, Okamoto Y, Tokunaga S, Zhu L, Shen H, Takashima H (2012). Alanyl-tRNA synthetase mutation in a family with dominant distal hereditary motor neuropathy. Neurology 78:1644–1649.

Zhu D, Kennerson ML, Walizada G, Züchner S, Vance JM, Nicholson GA (2005). Charcot-Marie-Tooth with pyramidal signs is genetically heterogeneous: families with and without MFN2 mutations. Neurology 65:496–497.

Case Report

Korean J Anesthesiol 2014 November 67(5): 346-349
http://dx.doi.org/10.4097/kjae.2014.67.5.346

# Pulmonary alveolar hemorrhage from a pulmonary artery false aneurysm after Swan-Ganz catheterization in a thoracic aortic aneurysm patient
## -a case report-

Daisuke Sugiyama[1,4], Shigeo Ikeno[1], Tetsuya Tsuchihashi[1], Shigeru Yokota[1], Hiroaki Ina[1], Tetsuya Kono[2], Kunihiko Yamashita[3], and Mikito Kawamata[4]

Departments of [1]Anesthesia, [2]Cardiovascular Surgery, [3]Radiology, Japanese Red Cross Society of Suwa Hospital, Suwa, [4]Department of Anesthesiology and Resuscitology, Shinshu University School of Medicine, Matsumoto, Japan

Pulmonary artery (PA) rupture caused by a PA Swan-Ganz catheter is a rare complication but remains fatal in almost 50% of cases. False aneurysm of the PA is a rare presentation of PA rupture and should be considered as a possible diagnosis in a patient with a new lung mass after PA catheterization. We present a case of sudden-onset pulmonary alveolar hemorrhage during cardiovascular surgery due to a traumatic PA false aneurysm. The Swan-Ganz catheter might have been displaced by the thoracic aortic aneurysm with displacement of the catheter causing the false aneurysm and bleeding. (Korean J Anesthesiol 2014; 67: 346-349)

**Key Words:** False aneurysm, Pulmonary artery, Swan-Ganz catheterization.

Pulmonary artery (PA) rupture, a rare complication of flow-directed PA Swan-Ganz catheterization, is estimated to occur at a frequency of 0.05 to 0.2% [1-3]. The mortality rate associated with this severe complication is estimated to be 40–50% [4]. Death is usually due to massive hemoptysis [2]. False aneurysm of the PA is a rare presentation of PA rupture and should be considered as a possible diagnosis in a patient with a new lung mass after PA catheterization [5]. Here, we present a case of sudden-onset pulmonary alveolar hemorrhage during cardiovascular surgery, due to a traumatic PA false aneurysm. The Swan-Ganz catheter might have been displaced by the thoracic aortic aneurysm with displacement of the catheter causing the false aneurysm and bleeding.

## Case Report

A 77-year-old woman, 156 cm in height and weighing 55 kg, was diagnosed as having angina pectoris and aneurysm of the thoracic aorta, and she was scheduled to undergo coronary artery bypass grafting and aortic arch replacement. She had been

Received: April 25, 2013. Revised: 1st, July 8, 2013; 2nd, July 10, 2013. Accepted: July 12, 2013.
Corresponding author: Daisuke Sugiyama, M.D., Department of Anesthesia, Japanese Red Cross Society of Suwa Hospital, 5-11-50, Kogandori, Suwa 392-8510, Japan. Tel: 81-266526111, Fax: 81-266576036, E-mail: sugidai@shinshu-u.ac.jp
This is an open-access article distributed under the terms of the Creative Commons Attribution Non-Commercial License (http://creativecommons.org/licenses/by-nc/3.0/), which permits unrestricted non-commercial use, distribution, and reproduction in any medium, provided the original work is properly cited.

Copyright © the Korean Society of Anesthesiologists, 2014

a smoker for more than 50 years and had also been diagnosed as having chronic obstructive pulmonary disease (COPD) complicated by PA hypertension. The patient was receiving treatment with oral diltiazem hydrochloride (100 mg/day) and furosemide (20 mg/day), and mean preoperative PA pressure was 20–30 mmHg. Preoperative laboratory tests revealed no coagulation abnormalities or any other notable abnormalities. At surgery, anesthesia was induced with propofol (80 mg), fentanyl (200 μg) and muscle relaxation with rocuronium (40 mg), and tracheal intubation was performed using a normal endotracheal tube (7 mm in internal diameter; Parker Flex-Tip™, Parker Medical, USA). No marked circulatory variations or abnormalities were observed during the induction of the general anesthesia. Anesthesia was maintained with 40% of oxygen, propofol (target-controlled infusion: 2.0 μg/ml), and remifentanil (0.2 μg/kg/min). A central venous catheter and a PA Swan-Ganz catheter were placed via the right internal jugular vein prior to the start of the surgery. The PA Swan-Ganz catheter was advanced up to the PA while the pressure waveforms were checked under the guidance of transesophageal echocardiography, and it was fixed at 40 cm after 1 cm was pulled out confirming wedging of the catheter tip in the PA. PA pressure after Swan-Ganz catheter insertion was 22 mmHg (mean), and pulmonary capillary wedge pressure was 18 mmHg.

Maximum airway pressure suddenly increased to 26 $cmH_2O$ from 15 $cmH_2O$ 30 minutes after the beginning of surgery, when the internal carotid artery graft was being secured for the coronary artery bypass. Endotracheal hemorrhage was detected, and the tracheal tube became filled and occluded with blood. There had been no change in wedge waveform of the PA Swan-Ganz catheter before the bleeding occurred. Ventilation was disrupted for 3 minutes with a transient fall of $SpO_2$ to 86%. However, positive pressure ventilation was maintained at airway pressures as high as 20 to 30 $cmH_2O$ with positive end-expiratory pressure (PEEP: 6 $cmH_2O$) while suction of the blood filling the tracheal tube was performed, and the bleeding ceased 15 minutes after it had been detected. Bronchoscopic observation revealed numerous clots in the tracheal tube, with complete occlusion of the right main bronchus. A total of 300 ml of blood was aspirated from the airway. As continuation of the surgery was deemed impossible, the surgery was suspended and the patient was admitted to the intensive care unit (ICU) with the tracheal tube in place.

A postoperative chest X-ray showed decreased lucency of the

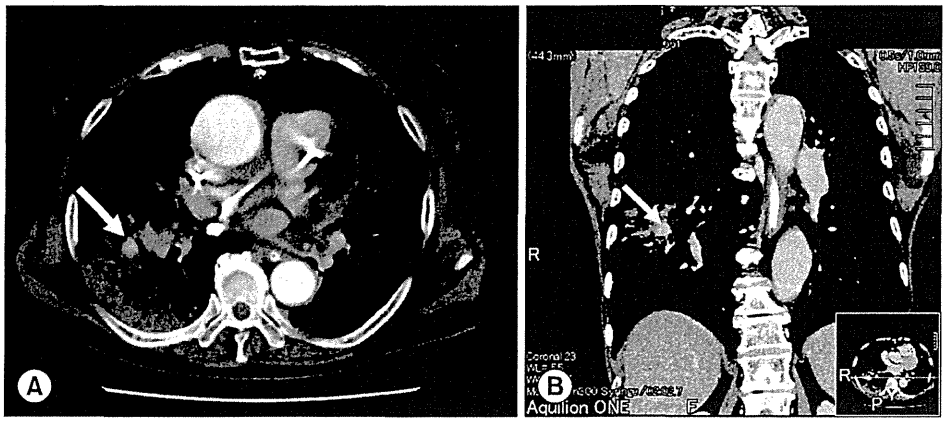


**Fig. 1.** Chest CT just after surgery in the transverse section (A) and coronal section (B). CT revealed a contrast-enhanced false aneurysm measuring 2 cm in diameter in the right PA. Arrow indicates a contrast-enhanced false aneurysm.

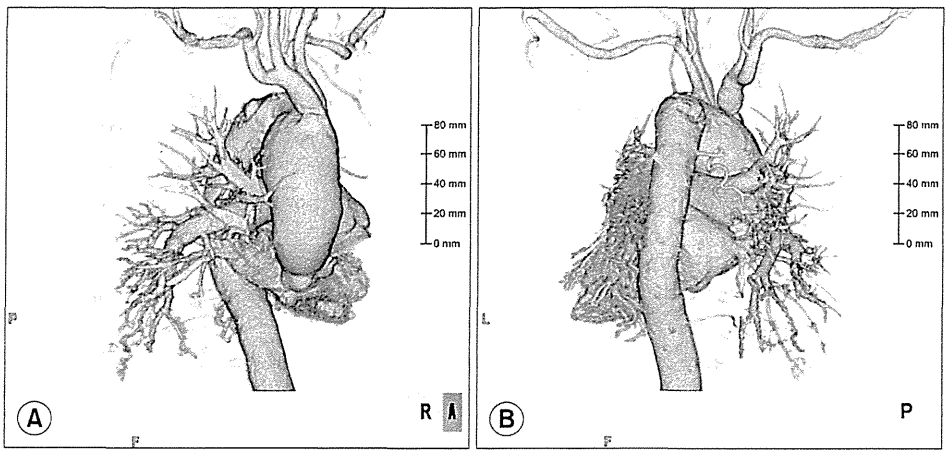


**Fig. 2.** Reconstructive 3D visualization from the presurgical CT scan: (A) anteroposterior view, and (B) posteroanterior view. The right main pulmonary artery was pressed by the thoracic artery aneurysm (arrow).

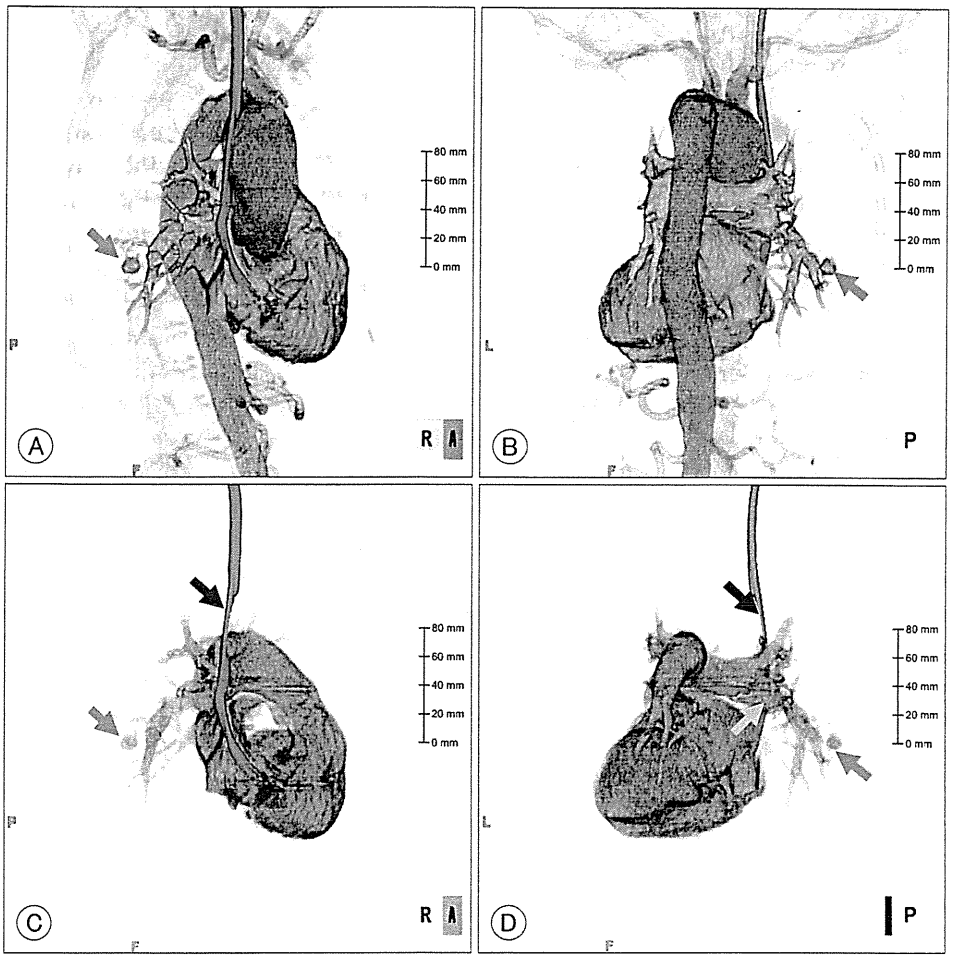


**Fig. 3.** Reconstructive 3D visualization from the postsurgical CT scan: (A) anteroposterior view, (B) posteroanterior view, (C) anteroposterior view without the aorta, and (D) posteroanterior view without the aorta. The PA Swan-Ganz catheter had shifted at the thoracic artery aneurysm level (black arrow). The tip of the PA Swan-Ganz catheter was maintained at a distance from the PA aneurysm (red and yellow arrows).

right lower lung field. Chest CT revealed a contrast-enhanced false aneurysm measuring 2 cm in diameter in the right PA (Fig. 1). Conservative treatment by mechanical ventilation with applied PEEP (6–8 $cmH_2O$) was selected over invasive treatment because the false aneurysm was small in size and bleeding from the aneurysm had ceased. Retrospectively, chest 3D CT images were confirmed (Fig. 2). The right main PA was pressed by the thoracic aortic aneurysm. A chest 3D CT after surgery revealed that the PA Swan-Ganz catheter had shifted at the thoracic artery aneurysm level (Fig. 3). The tip of the PA Swan-Ganz catheter was maintained at a distance from PA aneurysm (Fig. 3). A repeat chest X-ray and CT on the 16th postoperative day revealed improvement, and the contrast-enhanced false PA aneurysm could no longer be visualized. The patient's respiratory condition also improved, and she was extubated and discharged from the ICU on the 20th postoperative day.

## Discussion

A PA Swan-Ganz catheter is usually implanted via the right internal jugular vein. Since a PA Swan-Ganz catheter introduced via the right internal jugular vein is likely to be placed in the right PA, iatrogenic trauma caused by the placement of this catheter involves the middle and inferior lobar branches of the right PA in approximately 90% of cases [3], as in the present case. The risk factors for PA injury caused by PA catheterization include advanced age, pulmonary hypertension, anticoagulant therapy, hypothermia, faulty placement of the catheter, and faulty operation of the balloon [3]. Of these, advanced age and pulmonary hypertension associated with COPD were the relevant risk factors in our patient. The balloon was operated very carefully; however, the vulnerable blood vessel was probably damaged when the balloon was dilated and wedged into the artery, and pulmonary alveolar hemorrhage occurred due to the traumatic PA false aneurysm. Chest 3D CT images showed that the right main PA was pressed by the thoracic aortic aneurysm (Fig. 2). The chest 3D CT after surgery revealed that the PA Swan-Ganz catheter had shifted at the thoracic artery aneurysm level (Fig. 3). Therefore, there is a possibility that the tip of the PA Swan-Ganz catheter moved unexpectedly because of the existence of a thoracic aortic aneurysm, and the vulnerable blood vessel was damaged even though the PA Swan-Ganz catheter had been carefully

operated.

Routine treatment for hemoptysis during general anesthesia includes 100% oxygen, changes in position to the bleeding lung side down, changing the tube to a double lumen, and PEEP [3,4]. Useful interventions for the management of endotracheal hemorrhage caused by PA injury include occlusion of the airway on the side of the bleeding by differential lung ventilation, bronchoscopic hemostasis, ventilation with PEEP, hemostasis by endovascular treatment, lobectomy, and direct repair of the PA [6-10]. Hemostasis by endovascular treatment or surgical treatment such as lobectomy is considered when conservative treatment is difficult or when there is intrathoracic hemorrhage [1,3,6]. In our patient, hemostasis was achieved within a short time by the application of high PEEP, and airway patency and ventilation could fortunately be maintained, probably because of the very limited extent of injury and the small size of the false aneurysm of the PA as demonstrated by imaging.

In general, patients with endotracheal hemorrhage due to iatrogenic trauma caused by a PA catheter are considered to remain at a high risk of rebleeding even after hemostasis has been achieved by conservative treatment [1,3]. Rebleeding is often characterized by rapid and massive bleeding, and it is more serious. Rebleeding reportedly occurs within 48 hours in most cases, although there are reports of rebleeding occurring a few weeks or even a few months after the initial bleeding [1,3,6,8]. If respiratory management is undertaken with a normal endotracheal tube, prevention of rebleeding is an especially important consideration during treatment. In the present case, sufficient sedation with propofol and analgesia with fentanyl was provided after hemostasis in the ICU with close monitoring of the patient.

Our patient had been diagnosed as having COPD complicated by PA hypertension. COPD can cause a pulmonary artery aneurysm [2,11]. Therefore, our patient might have had pulmonary alveolar fragility before the surgery. PA injury caused by the placement of a PA Swan-Ganz catheter might have resulted in endotracheal hemorrhage, transiently disrupting ventilation; however, successful hemostasis could be achieved by conservative treatment using high PEEP, and the patient recovered. PA catheters are still frequently used in the perioperative period, especially for patients with decreased cardiac function and during cardiovascular surgical procedures [12]. Our case report raises the possibility of unexpected alveolar hemorrhage in a patient who has a thoracic aortic aneurysm due to a traumatic PA false aneurysm caused by placement of a PA Swan-Ganz catheter. PA Swan-Ganz catheters need to be operated with much caution, especially in a patient who has a thoracic artery aneurysm.

## References


1. McDaniel DD, Stone JG, Faltas AN, Khambatta HJ, Thys DM, Antunes AM, et al. Catheter-induced pulmonary artery hemorrhage. Diagnosis and management in cardiac operations. J Thorac Cardiovasc Surg 1981; 82: 1-4.
2. Shah KB, Rao TL, Laughlin S, El-Etr AA. A review of pulmonary artery catheterization in 6,245 patients. Anesthesiology 1984; 61: 271-5.
3. Urschel JD, Myerowitz PD. Catheter-induced pulmonary artery rupture in the setting of cardiopulmonary bypass. Ann Thorac Surg 1993; 56: 585-9.
4. Sirivella S, Gielchinsky I, Parsonnet V. Management of catheter-induced pulmonary artery perforation: a rare complication in cardiovascular operations. Ann Thorac Surg 2001; 72: 2056-9.
5. Ferretti GR, Thony F, Link KM, Durand M, Wollschläger K, Blin D, et al. False aneurysm of the pulmonary artery induced by a Swan-Ganz catheter: clinical presentation and radiologic management. AJR Am J Roentgenol 1996; 167: 941-5.
6. Carlson TA, Goldenberg IF, Murray PD, Tadavarthy SM, Walker M, Gobel FL. Catheter-induced delayed recurrent pulmonary artery hemorrhage. Intervention with therapeutic embolism of the pulmonary artery. JAMA 1989; 261: 1943-5.
7. Choong CK, Meyers BF. Lung mass after pulmonary artery catheterization: beware of the pulmonary artery false aneurysm. J Thorac Cardiovasc Surg 2005; 130: 899-900.
8. Feng WC, Singh AK, Drew T, Donat W. Swan-Ganz catheter-induced massive hemoptysis and pulmonary artery false aneurysm. Ann Thorac Surg 1990; 50: 644-6.
9. Olearchyk AS, Varada A. Perforation of the right pulmonary artery branch to the right middle lobe with a Swan-Ganz catheter during cardiopulmonary bypass, resulting in endobronchial hemorrhage. J Thorac Cardiovasc Surg 1991; 102: 807-8.
10. Urschel JD, Parrott JC. Repair of catheter-induced perforation of the pulmonary artery. Ann Thorac Surg 1991; 51: 1046.
11. Cherwek H, Amundson S. Images in clinical medicine. Pulmonary-artery aneurysm. N Engl J Med 2003; 348: e1.
12. Tempe DK, Gandhi A, Datt V, Gupta M, Tomar AS, Rajesh V, et al. Length of insertion for pulmonary artery catheters to locate different cardiac chambers in patients undergoing cardiac surgery. Br J Anaesth 2006; 9: 147-9.

## LETTER TO THE EDITOR

# SUCCESSFUL INTUBATION USING MCGRATH® MAC IN A PATIENT WITH TREACHER COLLINS SYNDROME

TAKATOSHI TSUJIMOTO*, SATOSHI TANAKA**, YUKI YOSHIYAMA*, YUKI SUGIYAMA*** AND MIKITO KAWAMATA****

Treacher Collins syndrome (TCS) is a congenital malformation of craniofacial development, which is associated with difficult tracheal intubation[1]. Several video laryngoscopes that have recently been developed have been shown to improve the laryngeal view in pediatric patients with difficult airways, including patients with TCS[2-4]. McGRATH® MAC (MAC; Aircraft Medical, Edinburgh, UK) has more recently been developed as a new video laryngoscope modified from McGRATH® Series 5 and may provide a better view of the glottis for intubation in adult patients[5]. However, there has been no report on the usefulness of MAC for intubation in pediatric patients with difficult airways.

A 13-year-old boy (146 cm; 36 kg) with TCS was scheduled for exotropia surgery under general anesthesia. Tetralogy of Fallot repair had been performed at the age of 4 years, when the trachea was intubated using a Macintosh laryngoscope despite Cormack-Lehane classification grade 3. At the age of 11 years, when mandibular distraction osteogenesis was performed, fiberoptic scope-guided endotracheal intubation was accomplished after failure of intubation using a Macintosh laryngoscope at a regional hospital. The patient showed the characteristic facial appearance of TCS such as micrognathia **(Fig. 1-A)**. Thyromental and interincisor distances were 40 mm and 18 mm, respectively, showing moderate trismus. A magnetic resonance imaging scan revealed a relatively long distance from the mouth to the larynx **(Fig. 1-B)**. Since we considered the airway to be patent in this patient under mask ventilation, general anesthesia was induced with 70 mg of propofol after setting up alternative devices to secure the airway, including equipment for percutaneous tracheostomy and a transtracheal jet ventilator. After mask ventilation has been successfully achieved, neuromuscular block was induced with 20 mg of rocuronium. In order to check the difficult airway in this patient, we used a Macintosh blade no. 3 and failed to visualize the epiglottis, defined as Cormack-Lehane classification grade 4. An attempt was then made to intubate using MAC with blade no. 3 **(Fig. 1-C)**. The blade was easily inserted into the larynx and exposed the epiglottis and the vocal cord, defined as Cormack-Lehane classification grade 1. The trachea was successfully intubated with an ID 6.0 mm tracheal tube without difficulty.

* MD, Resident anesthesiologist.
** MD, Assistant Professor.
*** MD, Instructor.
**** MD, Professor and Chairman.
Affiliation: Department of Anesthesiology and Resuscitology, Shinshu University School of Medicine.
**Corresponding author:** Dr. Mikito Kawamata, Department of Anesthesiology and Resuscitology, Shinshu University School of Medicine, 3-1-1, Asahi, Matsumoto, Nagano 390-8621, JAPAN. Tel: +81-263-37-2670, Fax: +81-263-35-2734. E-mail: kawamata@shinshu-u.ac.jp

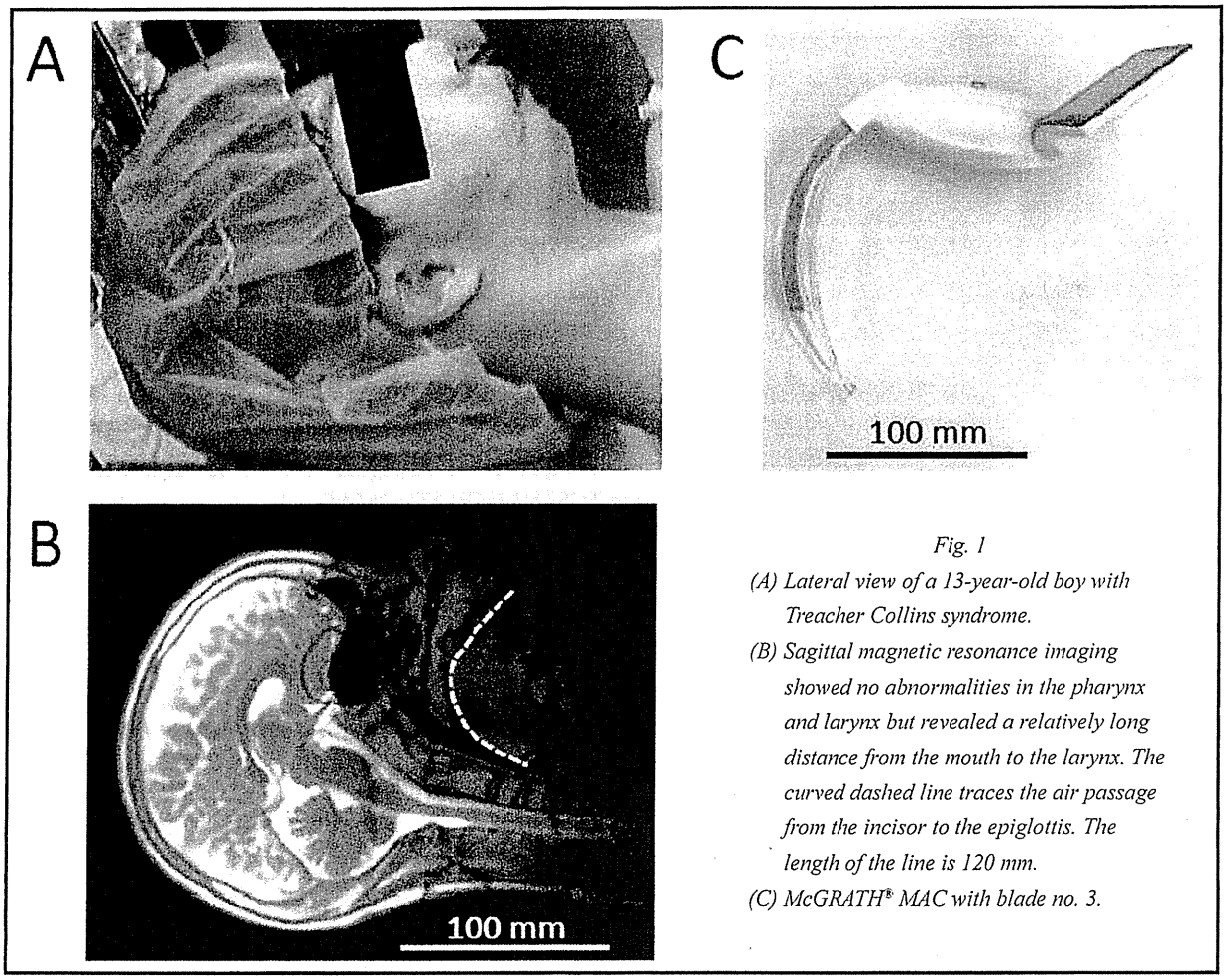


*Fig. 1*
*(A) Lateral view of a 13-year-old boy with Treacher Collins syndrome.*
*(B) Sagittal magnetic resonance imaging showed no abnormalities in the pharynx and larynx but revealed a relatively long distance from the mouth to the larynx. The curved dashed line traces the air passage from the incisor to the epiglottis. The length of the line is 120 mm.*
*(C) McGRATH® MAC with blade no. 3.*

Video-laryngoscopes such as the GlideScope®, Glidescope Cobalt® (Verathon Medical Inc., Bothell, WA, USA) and Pentax-Airway Scope ® (AWS; Hoya Co., Tokyo, Japan) have been reported to be useful for tracheal intubation in patients with difficult airways[2-4]. However, the usefulness of video laryngoscopes differs in patients with difficult airways, depending on features and severity of their anatomical abnormality in the oral cavity, pharynx and larynx[6]. Features of TCS include micrognathia, small mouth, high arched palate, cleft palate and velopharyngeal incompetence, and tracheal intubation becomes difficult with advance of age[1]. In this patient, blade no. 3 of MAC could easily reach the larynx and visualize the glottis and vocal cord. This is probably because the shape of the blade of MAC fitted to the oropharyngeal features in this patient. Thus, the McGrath MAC may be useful for tracheal intubation in pediatric patients who have micrognathia and a small mouth as were seen in this patient.

## References


1. HOSKING J, ZOANETTI D, CARLYLE A, ANDERSON P, COSTI D: Anesthesia for Treacher Collins syndrome: a review of airway management in 240 pediatric cases. *Pediatr Anesth*; 2012, 22:752-8.
2. LEE JH, PARK YH, BYON HJ, HAN WK, KIM HS, KIM CS, KIM JT: A comparative trial of the GlideScope® video laryngoscope to direct laryngoscope in children with difficult direct laryngoscopy and an evaluation of the effect of blade size. *Anesth Analg*; 2013, 117:176-81.
3. IGUCHI H, SASANO N, SO M, HIRATE H, SASANO H, KATSUYA H: Orotracheal intubation with an Airway Scope in a patient with Treacher Collins syndrome. *J Anesth*; 2008, 22:186-8.
4. ILIES C, FUDICKAR A, THEE C, DÜTSCHKE P, HANSS R, DOERGES V, BEIN B: Airway management in pediatric patients using the Glidescope Cobalt®: a feasibility study. *Minerva Anestesiol*; 2012, 78:1019-25.
5. HEALY DW, MATIES O, HOVORD D, KHETERPAL S: A systematic review of the role of videolaryngoscopy in successful orotracheal intubation. *BMC Anesthesiol;* 2012, 12:32. http://www.biomed-entral.com/ 1471-2253/12/32.
6. HYUGA S, SEKIGUCHI T, ISHIDA T, YAMAMOTO K, SUGIYAMA Y, KAWAMATA M: Successful tracheal intubation with the McGrath® MAC video laryngoscope after failure with the Pentax-AWS™ in a patient with cervical spine immobilization. *Can J Anaesth*; 2012, 59:1154-5.

# Calcitonin Gene–related Peptide Is Involved in Inflammatory Pain but Not in Postoperative Pain

Kumiko Ishida, M.D., Tomoyuki Kawamata, M.D., Satoshi Tanaka, M.D., Takayuki Shindo, M.D., Mikito Kawamata, M.D.

## ABSTRACT

**Background:** The aim of this study was to clarify the roles of calcitonin gene–related peptide (CGRP) in postoperative pain and inflammatory pain.

**Methods:** αCGRP knockout mice that the authors have developed and wild-type mice were used. Pain behaviors were assessed after incision and complete Freund's adjuvant (CFA) injection. Changes in CGRP and c-Fos expression in the dorsal horn were also examined.

**Results:** Guarding pain scores in αCGRP knockout mice were lower than those in wild-type mice at 24 h (3.8 ± 1.6 *vs.* 6.8 ± 1.5, $P = 0.044$) and 48 h (1.8 ± 1.7 *vs.* 6.0 ± 1.5, $P = 0.001$) after CFA injection (n = 8 to 9). Withdrawal latencies to heat stimulation in αCGRP knockout mice were higher than those in wild-type mice at 24 to 72 h after CFA injection (4.9 ± 1.0 *vs.* 3.4 ± 0.8 at 24 h, $P = 0.04$; 5.1 ± 0.3 *vs.* 3.2 ± 0.9 at 48 h, $P = 0.047$; and 5.4 ± 1.6 *vs.* 3.5 ± 0.5 s at 72 h, $P = 0.045$) (n = 11 to 13), but withdrawal thresholds to mechanical stimulation were comparable. CGRP expression was increased at 24 h after CFA injection in wild-type mice, and the c-Fos–positive profile was increased at 4 h after CFA injection (ipsilateral *vs.* contralateral: 12.3 ± 4.6 *vs.* 1.3 ± 1.9, $P < 0.0001$) and maintained at 24 h (10.0 ± 4.1 *vs.* 0.8 ± 1.3, $P < 0.0001$) (n = 4 to 6).

**Conclusion:** These results suggest that contribution of the αCGRP system depends on the modality of pain and the stage of inflammation. **(ANESTHESIOLOGY XXX; XXX:XXX-XX)**

TO better understand the mechanisms of pain and to develop new pain treatments, much effort has been spent developing and analyzing preclinical models of pathophysiological pain. A postoperative pain model and an inflammatory pain model have been widely used to understand the pathophysiological pain associated with tissue injury and inflammation. These two pain models share common behavioral phenotypes as acute pain including spontaneous pain, thermal hyperalgesia, and mechanical hyperalgesia.[1,2] However, recent studies have shown that the mechanisms of postoperative pain are different from those of inflammatory pain.[2]

Calcitonin gene–related peptide (CGRP), which is a 37-amino-acid neuropeptide widely distributed in the peripheral and central nervous systems, is a member of a family of structurally and biologically related polypeptides, including adrenomedullin, amylin, calcitonin, and calcitonin receptor–stimulating peptide. CGRP exists as α and β isoforms that are derived from different genes.[3] αCGRP is abundantly expressed in dorsal root ganglion (DRG) neurons, whereas βCGRP coexists with αCGRP in DRG neurons at a much lower expression level than that of αCGRP.[4] Because CGRP has long been served as a molecular marker of peptidergic nociceptive neurons,[5] CGRP has been expected to play an important role in pathophysiological nociceptive pain. Actually, in calcitonin/αCGRP knockout mice, intraarticular carrageenan/kaolin-induced thermal hyperalgesia was significantly inhibited, suggesting that αCGRP is involved in thermal hyperalgesia in joint inflammation.[6] In addition, spinal administration of a CGRP receptor antagonist, $CGRP_{8-37}$, inhibited hyperalgesia after inflammation

### What We Already Know about This Topic

- Inflammatory and incisional pain share several pain-related phenotypes, but may have different underlying signaling mechanisms.

### What This Article Tells Us That Is New

- Mice deficient in the α isoform of calcitonin gene–related peptide (CGRP) display reduced pain-related behaviors after the injection of complete Freund's adjuvant (CFA). No CGRP-related differences were observed after incision. CGRP-deficient mice also had reduced spinal cord Fos expression after CFA injection.
- These data distinguish incision- and inflammation-related pain on a biochemical level.

Submitted for publication November 9, 2013. Accepted for publication June 6, 2014.

From the Department of Anesthesiology and Resuscitology, Shinshu University School of Medicine, Matsumoto, Japan (K.I., T.K., S.T., M.K.); and Department of Cardiovascular Research, Shinshu University Graduate School of Medicine, Matsumoto, Japan (T.S.).

*Copyright © 2014, the American Society of Anesthesiologists, Inc. Lippincott Williams & Wilkins.* Anesthesiology 2014; XXX:00-00



Copyright © by the American Society of Anesthesiologists. Unauthorized reproduction of this article is prohibited.

ezdoi;10.1097/ALN.0000000000000364

and spinal cord injury, suggesting that spinal CGRP is involved in hyperalgesia.[7,8] However, it remains to be elucidated in which types of pathophysiological nociceptive pain, postoperative pain and/or inflammatory pain, CGRP is involved. It has also not been elucidated in which modalities of pathophysiological pain CGRP is involved.

We hypothesized that the CGRP-related systems differentially contribute to the development of various types of pain such as inflammatory pain and postoperative pain. We have originally developed αCGRP knockout mice in which αCGRP but not calcitonin is depleted.[9] The aim of this study was thus to clarify the roles of αCGRP in the two types of pathophysiological nociceptive pain using αCGRP knockout mice.

## Materials and Methods

All the protocols of this study were approved by the Animal Care and Use Committee of Shinshu University School of Medicine, Matsumoto, Japan (reference No. 09-015). Mice were treated in accordance with the Ethics Guidelines for Investigations of Experimental Pain in Conscious Animals as issued by the International Association for the Study of Pain. Every effort was made to minimize animal suffering and to reduce the number of animals used in this study.

### Animals

We used male αCGRP knockout mice weighing 25 to 30 g with the genetic background of the 129SV × C57BL/6 hybrid as we previously reported[9] and their male wild-type (WT) littermate controls. αCGRP knockout mice are healthy, show normal behavior, and have no visible phenotype different from that of normal mice.[10] Mice housed in groups of four animals were maintained on a 12-h light–dark cycle with food and water available *ad libitum*.

### Animal Models of Pain

Mice were randomly divided by computer-generated randomization into two groups, incision or complete Freund's adjuvant (CFA; Sigma, St. Louis, MO) injection. Mice were anesthetized with 2 to 3% halothane in 100% oxygen. To make a postoperative pain model, a plantar incision was made according to a modification of a previous report.[11] In brief, a 6-mm longitudinal incision was made with a number 11 blade through the skin, fascia, and muscle of the right hind paw. The skin was apposed with two single sutures of 7-0 nylon. The wound was covered with antibiotic ointment.

In another series of experiments, mice received a subcutaneous injection of 20 μl of CFA to make an inflammatory pain model. In brief, during anesthesia with 2 to 3% halothane in 100% oxygen, CFA or a vehicle (0.9% saline) was injected in the plantar surface of the right hind paw using a Hamilton syringe with a 30-gauge needle. After both types of injury, anesthesia was discontinued and mice were allowed to recover in their cages.

### Assessment of Paw Edema

The degree of edema, which is the indicative of the intensity of inflammation, was evaluated by measuring the paw thickness according to a previously described method.[1] The maximal dorso-ventral thickness of the paw was measured using calipers before and 2, 4, 6, and 24 h after incision or CFA injection.

### Behavioral Testing

To habituate mice to the testing environment, they were acclimated for 2 days. The basal value in each behavioral test before incision or CFA injection was obtained on the third day. The following behavioral tests were performed for each paw before and 2, 4, 6, 24, 48, 72, 120, and 168 h after incision or CFA injection. The person performing the following tests was blinded to the treatment and genotypes of mice.

The guarding pain score (GPS) of the hind paws was calculated to assess the spontaneous pain-related behavior according to a previously described method.[12] Unrestrained mice were placed on a stainless steel mesh floor (openings, 8 × 8 mm) under a clear plastic cage and allowed to acclimate for 15 min. GPS was calculated on the basis of weight bearing. Both paws of each animal were closely observed during a 1-min period repeated every 5 min for 30 min. Depending on the position in which the paw was found during the scoring period, a score of 0, 1, or 2 was given. Full weight bearing on the paw (score = 0) was present if the wound was blanched or distorted by the mesh. If the area of the wound touched the mesh without blanching or distorting, a score of 1 was given. If the paw was completely off the mesh, a score of 2 was recorded. The sum of six scores (0 to 12) was used to assess the pain in the incised or CFA-injected paw.

Mice were placed on a stainless mesh floor covered with a clear plastic cage top. For testing mechanical responses, calibrated von Frey filaments were applied adjacent to the wound in unrestrained mice. We determined the 50% mechanical withdrawal threshold (MT) by the "up–down method" according to a previous report.[13] A series of seven von Frey filaments (0.7-, 1.6-, 4-, 6-, 10-, 14-, and 20-mN forces) were used. Testing was initiated with 6 mN forces. Whenever a positive response occurred, the next weaker von Frey filament was applied. Whenever a negative response occurred, the next stronger one was applied. The test was continued until the response of six stimuli after the first change in response had been obtained or the test reached either end of the spectrum of the von Frey set. MT was calculated by using the formula by Chaplan *et al.*[13]: 50% MT = $(10^{[Xf + k\delta]})/10{,}000$, where Xf = value (in log units) of the final von Frey filament used; k = tabular values for the pattern of positive/negative responses; and δ = mean difference (in log units) between stimuli (here, 0.22).

Paw withdrawal latency (PWL) to noxious heat stimuli was assessed by applying a focused radiant heat source (model number 37370; Ugo Basil, Comerio, Italy) to unrestrained



Copyright © by the American Society of Anesthesiologists. Unauthorized reproduction of this article is prohibited.

mice. The latency to evoke a withdrawal response was determined with a cutoff value of 20 s to avoid tissue damage. The intensity of the heat was adjusted so that the basal PWL was 10 to 15 s in WT mice.

In a separate study, to determine through which site (spinal or peripheral) CGRP contributes to the CFA-induced inflammatory pain, mice were randomly divided into seven groups. These groups were given intraplantar administration of $CGRP_{8-37}$ (Peptide Institute Inc., Osaka, Japan) at doses of 0.05, 0.5, and 5 nmol in 20 μl saline or intrathecal administration of $CGRP_{8-37}$ at doses of 0.005, 0.05, and 0.5 nmol in 10 μl of saline or a vehicle. The person performing the behavioral experiments was blinded to the drug and dose. A Hamilton syringe attached to a 30-gauge needle was used for intrathecal or intraplantar administration. $CGRP_{8-37}$ was intrathecally administered *via* the interspace between L4 and L5 vertebrae according to a previously described method.[14] For intraplantar administration, $CGRP_{8-37}$ was injected into the right hind paw where CFA had been injected. PWLs to noxious heat stimuli were assessed before and 10, 20, 30, 45, and 60 min after intrathecal or intraplantar administration.

After behavioral tests, some animals were used for subsequent immunohistochemical studies. The remaining animals were euthanized 7 days after incision or CFA injection.

### *Immunohistochemical Studies*

In both αCGRP knockout mice and WT mice, some naive animals were just anesthetized with 2 to 3% halothane in 100% oxygen without incision or CFA injection and considered as "controls." We used polyclonal antibodies raised against the following molecules: αβCGRP (1:8,000, C8198, rabbit; Sigma), c-Fos (1:20,000, PC38; rabbit; Merck, Darmstadt, Germany), and protein kinase Cγ (PKCγ; 1:200, PKCg-Go-Af840, goat; Frontier Institute, Sapporo, Japan). Immunohistochemical analysis was conducted 4 and 24 h after incision and CFA injection. Mice were deeply anesthetized with 0.2 ml intraperitoneal urethane (0.24 g/ml) and perfused transcardially with 4% paraformaldehyde in 0.1-M phosphate buffer. The L4 to L5 segments of the spinal cord were removed. The spinal cord was immersed in 4% paraformaldehyde in phosphate buffer for 2 h for postfixation and then cryoprotected in 25% sucrose in phosphate-buffered saline (PBS) overnight at 4°C. The samples were placed in TissueTek embedding medium (Sakura, Tokyo, Japan) and rapidly frozen. The spinal cord was cut at 50-μm thickness using a sliding cryostat (Sakura). The following procedure was performed in a free-floating state. The tissue sections were washed in PBS and incubated for 1 h at room temperature in a blocking solution consisting of 10% normal donkey serum and 0.2% TritonX-100 (Sigma) in PBS (PBS-t). Sections were then incubated with a mixture of primary antibodies overnight at 4°C. After rinsing with PBS-t, the sections were incubated with Alexa Fluor 594-labeled and Alexa 647-labeled species-specific secondary antibodies at a dilution of 1:500 (Invitrogen, Carlsbad, CA) in PBS-t for 90 min at room temperature. Images were taken with a confocal laser scanning microscope (DIGITAL ECLIPSE C1; Nikon, Tokyo, Japan). In all cases, images were a single stack and were acquired with line-by-line sequential scanning to prevent bleed-through and cross-excitation of fluorophores.

Calcitonin gene–related peptide and c-Fos expression in the superficial dorsal horn (SDH) of the L4 to L5 segments was quantitatively analyzed according to the following method. The SDH (laminae I and II) was defined by the PKCγ-labeled area (fig. 1). Because the area labeled by PKCγ corresponds to the ventral part of lamina II in the mouse spinal cord,[15] the SDH was defined as the PKCγ-labeled area and the area dorsal to it in the dorsal horn. Four to six mice from each group were used for quantitative measurement of CGRP expression. Analyses were performed on five randomly selected sections from each animal. Images of sections were imported into Win Roof 6.1 software (Mitani, Fukui, Japan). Changes in CGRP staining were quantified using gray scales (0-black to 255-white). The relative intensity of the gray level was determined by dividing the gray level on the ipsilateral side to the treatment by that on the contralateral side in each pain model. The average relative

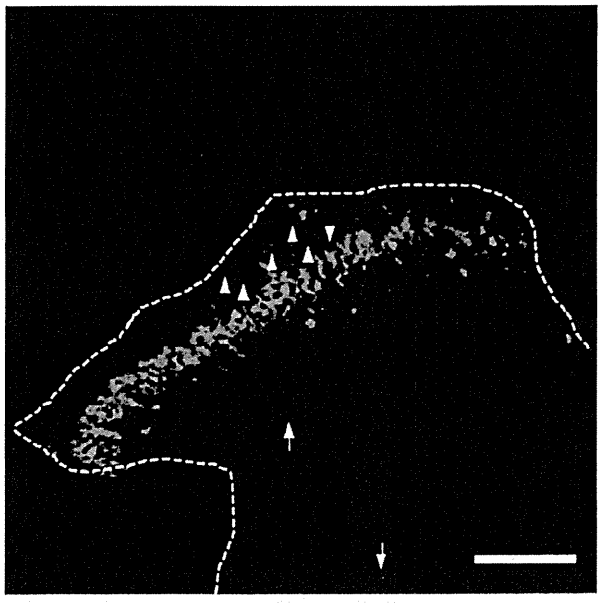

**Fig. 1.** Superficial dorsal horn (SDH) defined by protein kinase Cγ (PKCγ). The SDH of the L4 to L5 segments of the spinal cord was defined by the PKCγ-labeled area. Because the area labeled by PKCγ corresponds to the ventral part of lamina II in the mouse spinal cord, the SDH was defined as the PKCγ-labeled area and the area dorsal to it in the dorsal horn. *Green* and *red* indicate PKCγ and c-Fos immunoreactivities, respectively. The area surrounded by a *white dashed line* indicates the dorsal horn of the spinal cord. The area surrounded by a *red dashed line* indicates the SDH. *Arrowheads* and *arrows* indicate c-Fos–positive spinal neurons in the SDH and deep dorsal horn, respectively. *Scale bar* = 100 μm.



Copyright © by the American Society of Anesthesiologists. Unauthorized reproduction of this article is prohibited.

intensity (ipsilateral side/contralateral side) was calculated to determine the value for each animal. In naive mice, the relative intensity of the gray level was determined by dividing the gray level on the left side by that on the right side.

The number of c-Fos–positive neurons was counted in four to six mice from each group. Analyses were performed on six randomly selected sections from each animal. The number of c-Fos–positive neurons per section was calculated as the mean of six sections for each mouse.

A person who was blinded to the experimental design selected sections for each mouse, performed quantitative measurement of CGRP expression, and counted the number of c-Fos–positive neurons.

### Statistical Analysis

All statistical analyses were performed using GraphPad Prism software (GraphPad, San Diego, CA) and Ekuseru-toukei 2010 (Social Survey Research Information, Tokyo, Japan). Comparisons were performed using a two-tailed hypothesis testing. The sample size was based on previous similar studies.[6,16] Data are expressed as means ± SDs. For continuous data, normal distribution of values was determined by the Kolmogorov–Smirnov test. GPSs and PWLs were compared among the groups by two-way ANOVA for repeated measures with Tukey *post hoc* test. MT was presented as the median with first and third quartiles. Data for MT were analyzed using Friedman test for within-group analysis and the Kruskal–Wallis test for between-group comparisons followed by Dunnett *post hoc* test. PWLs after intrathecal or intraplantar injection of $CGRP_{8-37}$ were compared among groups by two-way ANOVA for repeated measures with Tukey *post hoc* test. Nonparametric data were analyzed with the Mann–Whitney U test or the Kruskal–Wallis test. To analyze the dose dependency of the effects of $CGRP_{8-37}$, the Jonckheere–Terpstra test was used. *P* value less than 0.05 was considered as statistically significant. No data for mice were lost during the experiment or were missed in the statistical analyses.

## Results

### Basal Responses to Noxious Mechanical and Heat Stimuli in αCGRP Knockout Mice

Basal MT to von Frey filaments in αCGRP knockout mice (1.8 [1.1 to 2.3], n = 13) was not significantly different from that in WT mice (1.5 [1.2 to 2.6], n = 13), and basal PWL to noxious heat stimuli in αCGRP knockout mice (10.4 ± 0.9 s, n = 18) was also not significantly different from that in WT mice (10.9 ± 1.6 s, n = 17). In addition, αCGRP knockout mice showed normal weight bearing.

### Paw Edema after Plantar Incision and CFA Injection

Paw thickness in αCGRP knockout mice was comparable with that in WT mice before incision and CFA injection (fig. 2). Plantar incision significantly increased the thickness of the incised paw, which was apparent 4 h after incision and lasted for at least 24 h in both αCGRP knockout mice and WT mice ($P < 0.05$, *vs.* 0 h; fig. 2A). Thickness of the incised paw in αCGRP knockout mice was comparable with that in WT mice throughout the observation period. CFA injection also increased the thickness of the injected paw in both αCGRP knockout mice and WT mice ($P < 0.05$, *vs.* 0 h; fig. 2B). Increased paw thickness was apparent 4 h after

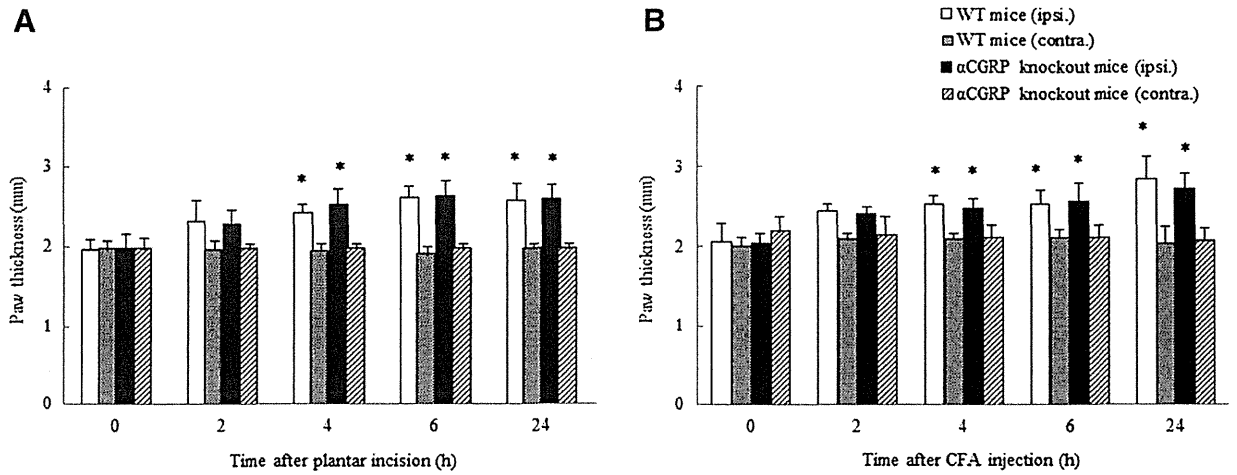


**Fig. 2.** Paw edema after incision and complete Freund's adjuvant (CFA) injection. (*A*) Time courses of changes in paw thickness in α-calcitonin gene–related peptide (αCGRP) knockout mice and wild-type (WT) mice before and after incision. (*B*) Time courses of changes in paw thickness in αCGRP knockout mice and WT mice before and after CFA injection. Paw thickness significantly increased from 4 h after incision and CFA injection and thereafter both in αCGRP knockout mice and WT mice compared with that before incision and CFA injection. However, there were no significant differences in paw thickness between αCGRP knockout mice and WT mice after incision and CFA injection. n = 5 or 6 in each group. Data are expressed as means ± SDs. *$P < 0.05$ compared with 0 h (baseline). Contralateral (contra.) = paw on the contralateral side to incision or CFA injection; ipsilateral (ipsi.) = paw on the ipsilateral side to incision or CFA injection.



Copyright © by the American Society of Anesthesiologists. Unauthorized reproduction of this article is prohibited.

incision and lasted for at least 24 h in both αCGRP knockout mice and WT mice. Thickness of the injected paw in αCGRP knockout mice was comparable with that in WT mice throughout the observation period. In both pain models, paw thickness on the contralateral side to the incision or CFA injection was not changed.

### *Involvement of αCGRP in Postoperative Pain*

Skin incision increased GPSs and decreased PWLs and MTs in both αCGRP knockout mice and WT mice. GPSs were significantly increased at 2, 4, and 6 h after incision compared with those before incision in both αCGRP knockout mice and WT mice ($P < 0.05$ in both types of mice, *vs.* 0 h; fig. 3A). There was no significant difference in GPS between αCGRP knockout mice and WT mice at each time point. PWLs and MTs were significantly decreased at 2 h after incision compared with those before incision in both types of mice ($P < 0.05$ in both types of mice; fig. 3, B and C). Significant decreases in PWLs and MTs were prolonged until 72 h after incision in both types of mice ($P < 0.05$, *vs.* 0 h). There was no significant difference in MT or PWL between αCGRP knockout mice and WT mice at each time point.

### *Involvement of αCGRP in Inflammatory Pain*

Complete Freund's adjuvant injection increased GPSs in both αCGRP knockout mice and WT mice. In WT mice, GPSs were significantly increased at 2 to 72 h after CFA injection compared with that before CFA injection ($P < 0.05$; fig. 4A). In αCGRP knockout mice, GPSs were significantly increased at only 2 to 24 h after CFA injection compared with that before CFA injection ($P < 0.05$; fig. 4A). Although GPSs in αCGRP knockout mice were comparable with those in WT mice at 2, 4, and 6 h after CFA injection, GPSs in αCGRP knockout mice were significantly lower than those in WT mice at 24 and 48 h after CFA injection ($P < 0.05$; fig. 4A).

Complete Freund's adjuvant injection decreased PWLs and MTs in both WT mice and αCGRP knockout mice. In WT mice, CFA injection significantly decreased PWLs at 2 to 168 h after CFA injection compared with that before CFA injection. In αCGRP knockout mice, PWLs were significantly

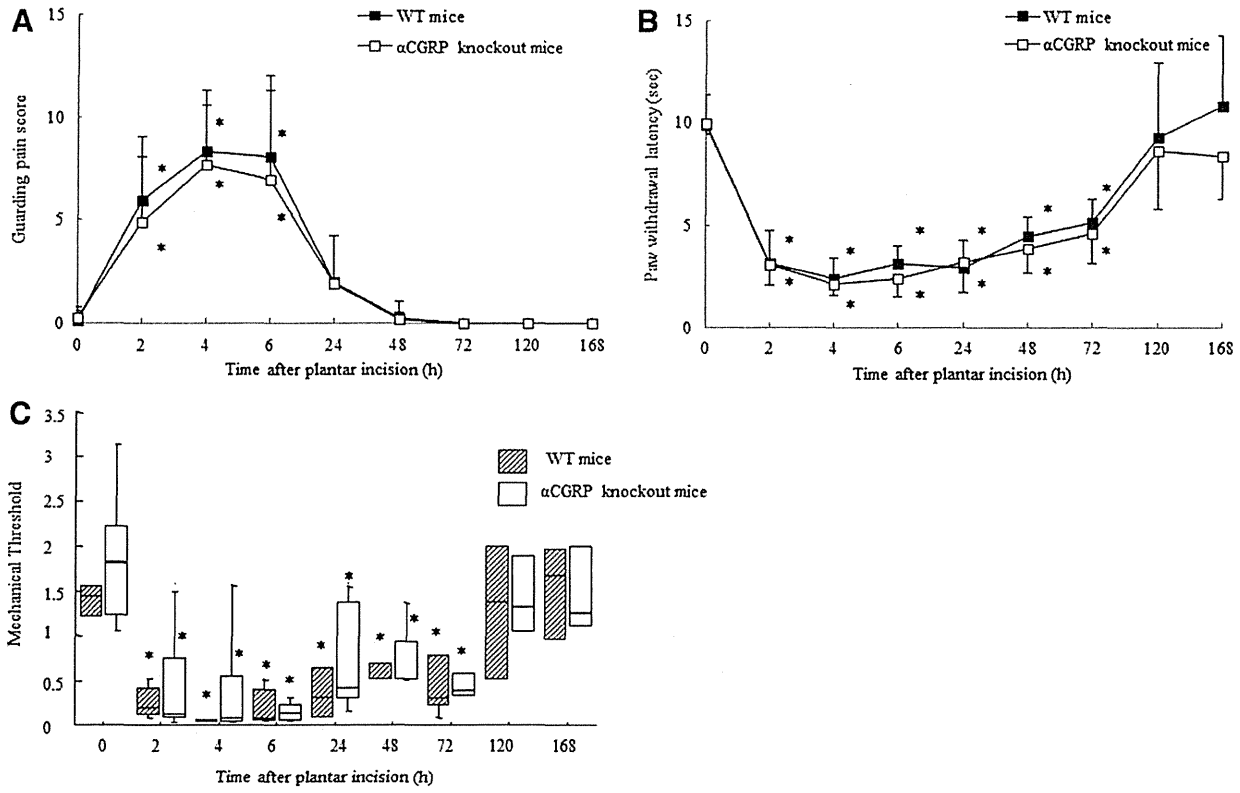


**Fig. 3.** Guarding pain score (GPS), paw withdrawal latency (PWL), and 50% mechanical withdrawal threshold (MT) after incision. (*A*) Time courses of GPSs after incision in α-calcitonin gene–related peptide (αCGRP) knockout mice and in wild-type (WT) mice. n = 12 in αCGRP knockout mice, n = 15 in WT mice. (*B*) Time courses of PWLs after incision in αCGRP knockout mice and WT mice. n = 6 in each group. (*C*) Time courses of MTs after incision in αCGRP knockout mice and WT mice. n = 6 in each group. GPSs were significantly increased at 2–6 h after incision, and PWLs and MTs were significantly decreased at 2–72 h after incision compared with those before incision in both αCGRP knockout mice and WT mice. There were no significant differences in GPSs, PWLs, and MTs between αCGRP knockout mice and WT mice at each time point. Data for GPS and PWL are expressed as means ± SDs. Data for MTs are expressed as medians (*horizontal line*) with 1st and 3rd quartiles (*boxes*) and 10th and 90th percentiles (*vertical lines*). *$P < 0.05$, *versus* 0 h (baseline).



Copyright © by the American Society of Anesthesiologists. Unauthorized reproduction of this article is prohibited.

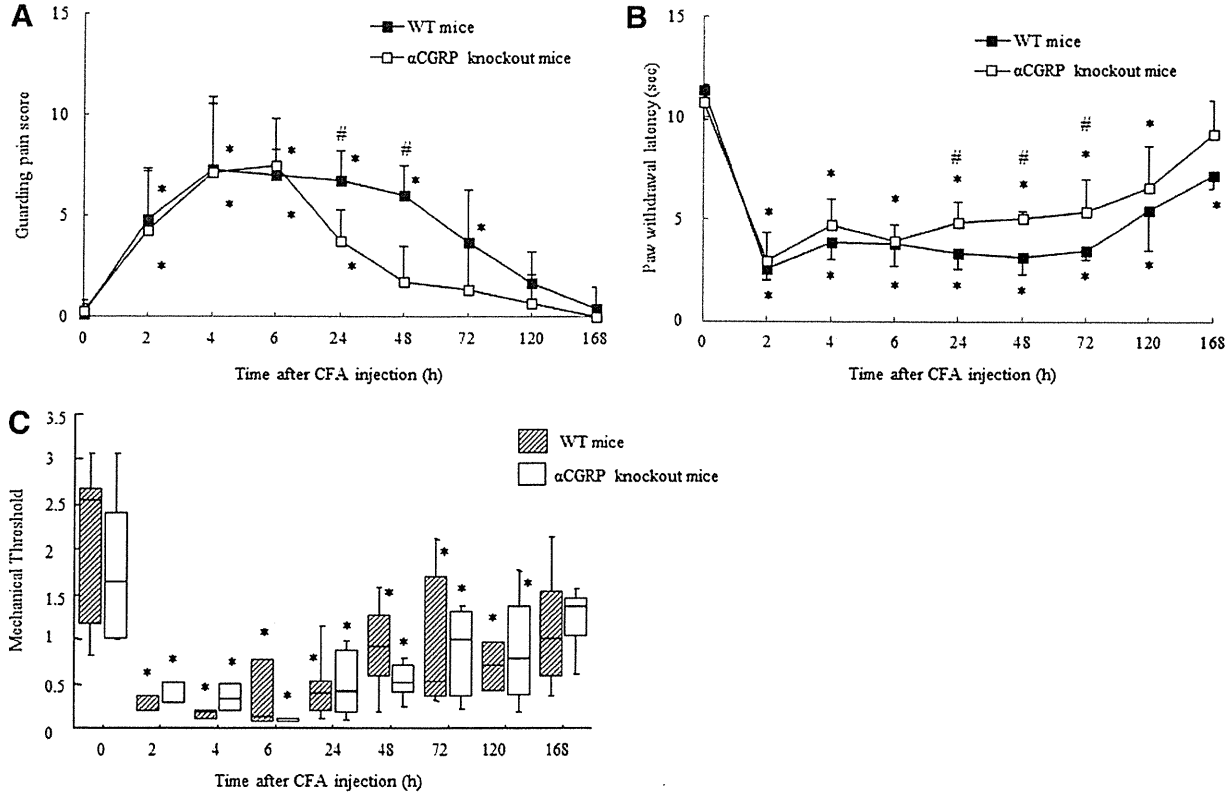


**Fig. 4.** Guarding pain score (GPS), paw withdrawal latency (PWL), and 50% mechanical withdrawal threshold (MT) after complete Freund's adjuvant (CFA) injection. (*A*) Time courses of GPSs in α-calcitonin gene–related peptide (αCGRP) knockout mice and in wild-type (WT) mice after CFA injection. n = 8 in αCGRP knockout mice, n = 9 in WT mice. (*B*) Time courses of PWLs in αCGRP knockout mice and WT mice after CFA injection. n = 13 in αCGRP knockout mice, n = 11 in WT mice. (*C*) Time courses of MTs in αCGRP knockout mice and WT mice after CFA injection. n = 7 in each group. In αCGRP knockout mice, GPSs were significantly increased at 2–24 h after CFA injection, but in WT mice, GPSs were significantly increased at 2–72 h after CFA injection compared with that before CFA injection. GPSs in αCGRP knockout mice were significantly lower than those in WT mice at 24 and 48 h after CFA injection. CFA injection significantly decreased PWLs at 2–120 h after CFA injection in αCGRP knockout mice and decreased PWLs at 2–168 h after CFA injection in WT mice compared with that before CFA injection. PWLs in αCGRP knockout mice were significantly longer than those in WT mice at 24–72 h after CFA injection. CFA injection also significantly decreased MTs at 2–120 h after CFA injection, compared with that before CFA injection, in both αCGRP knockout mice and WT mice. However, there was no significant difference in MT between αCGRP knockout mice and WT mice at each time point. Data for GPSs and PWLs are expressed as means ± SDs. Data for MTs are expressed as medians (*horizontal line*) with 1st and 3rd quartiles (*boxes*) and 10th and 90th percentiles (*vertical lines*). *$P < 0.05$, *versus* 0 h (baseline). #$P < 0.05$, αCGRP knockout mice *versus* WT mice.

decreased at 2 to 120 h after CFA injection compared with that before CFA injection ($P < 0.05$; fig. 4B). Although PWLs in αCGRP knockout mice were comparable with those in WT mice at 2, 4, 6, 120, and 168 h after CFA injection, PWLs in αCGRP knockout mice were significantly longer than those in WT mice at 24, 48, and 72 h after CFA injection ($P < 0.05$; fig. 4B). CFA injection also significantly decreased MTs at 2 to 120 h after CFA injection compared with that before CFA injection in both WT mice and αCGRP knockout mice ($P < 0.05$ in both types of mice; fig. 4C).

### *Effects of Intrathecal and Intraplantar Administration of $CGRP_{8-37}$ on Thermal Hyperalgesia in Inflammatory Pain*

To examine the site of action of CGRP, we examined the effects of intrathecal or intraplantar administration of the CGRP receptor antagonist $CGRP_{8-37}$ on decreased PWLs in WT mice after CFA injection. Twenty-four hours after CFA injection, $CGRP_{8-37}$ or a vehicle (saline) was administered. Intrathecal administration of $CGRP_{8-37}$ significantly reversed the decreased PWLs after CFA injection in a dose-dependent manner ($P < 0.001$; fig. 5, A and B). However, intraplantar administration of $CGRP_{8-37}$ did not have any effects on the decreased PWLs even at a dose of 5 nmol, which was 10 times higher than the highest dose (0.5 nmol) used in intrathecal administration (fig. 5C). Intrathecal and intraplantar administration of $CGRP_{8-37}$ did not affect PWLs of the paw on the contralateral side to CFA injection (data not shown). Intraplantar administration of 10 nmol $CGRP_{8-37}$ into the hind paw ipsilateral to the site of inflammation slightly reversed thermally decreased PWLs (from



Copyright © by the American Society of Anesthesiologists. Unauthorized reproduction of this article is prohibited.

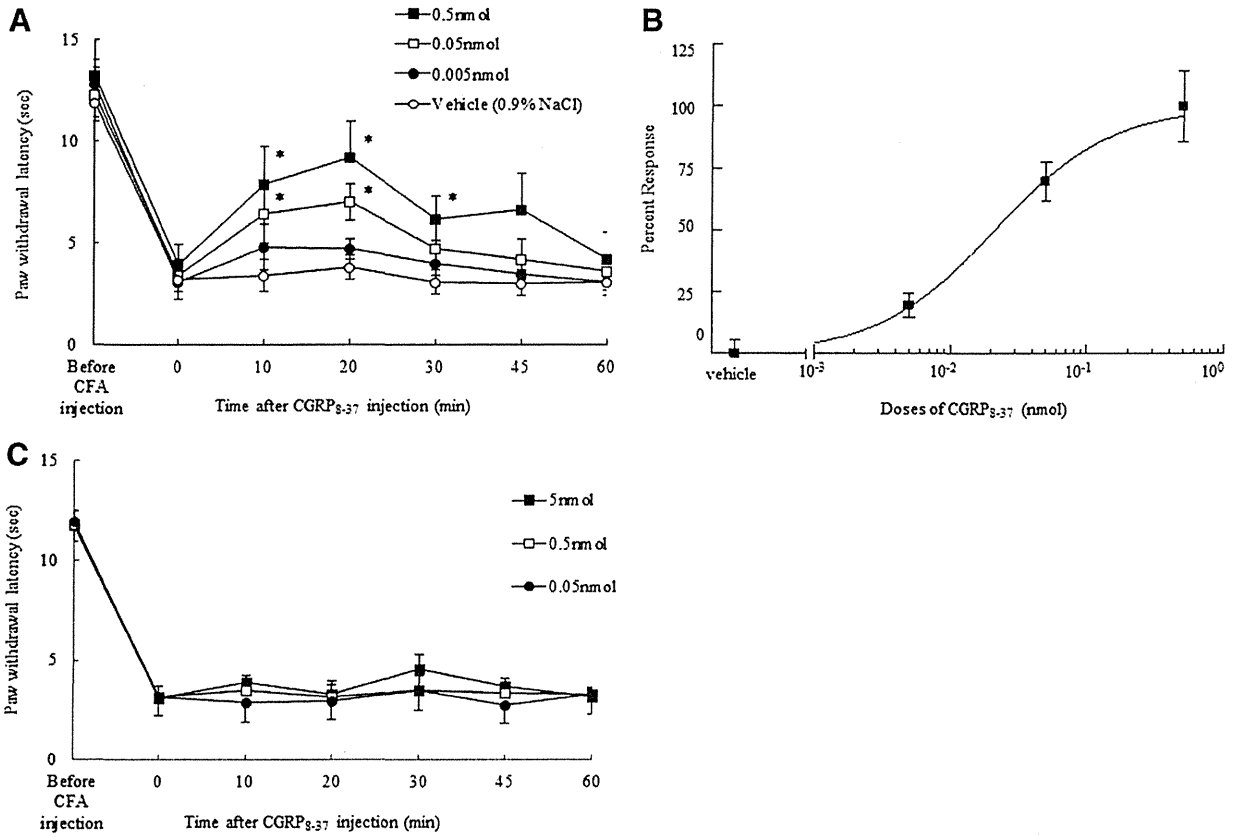


**Fig. 5.** Effects of intrathecal and intraplantar administration of calcitonin gene–related peptide (CGRP) antagonist on paw withdrawal latency (PWL) after complete Freund's adjuvant (CFA) injection. (*A*) Time courses of PWLs in wild-type mice after intrathecal administration of a CGRP receptor antagonist, $CGRP_{8-37}$. $CGRP_{8-37}$ (0.005, 0.05, or 0.5 nmol) or a vehicle was administered 24 h after CFA injection. n = 5 or 6 in each group. (*B*) Dose–response relationship of intrathecal $CGRP_{8-37}$. n = 5 or 6 in each group. (*C*) Time courses of PWLs in wild-type mice after intraplantar administration of $CGRP_{8-37}$. $CGRP_{8-37}$ (0.05, 0.5, or 5 nmol) was administered 24 h after CFA injection. n = 4 in each group. Intrathecal administration of $CGRP_{8-37}$ significantly reversed the decreased PWLs in a dose-dependent manner. Intraplantar administration of $CGRP_{8-37}$ did not have any effects on the decreased PWLs even at a dose of 5 nmol. Data are expressed as means ± SDs. *$P < 0.001$, *versus* vehicle.

3.8 ± 1.3 s to 5.4 ± 0.1 s). However, intraplantar administration of 10 nmol $CGRP_{8-37}$ into the contralateral hind paw also slightly reversed thermally decreased PWLs to the same degree as ipsilateral administration (from 3.9 ± 0.2 s to 5.5 ± 0.2 s). These results indicate that the antihyperalgesic effect of 10 nmol $CGRP_{8-37}$ was mediated systemically rather than locally. Therefore, we used $CGRP_{8-37}$ at a dose of 5 nmol as a maximal dose.

### *CGRP Expression in the SDH after Plantar Incision and CFA Injection*

Calcitonin gene–related peptide expression in the SDH was assessed in WT mice at 4 and 24 h after incision and CFA injection. Intense CGRP immunoreactivity was observed in the SDH in naive mice (fig. 6A), and the relative intensity of CGRP immunoreactivity (right side/left side) was 1.03 ± 0.21 (fig. 6B). CGRP immunoreactivity in the SDH on the ipsilateral side to the incision and CFA injection was not greatly increased at 4 h after incision and CFA injection, and the relative intensities of CGRP immunoreactivity at 4 h after incision and CFA injection were 1.01 ± 0.20 and 1.03 ± 0.18, respectively (fig. 6B). However, at 24 h after CFA injection, CGRP immunoreactivity in the SDH on the ipsilateral side to the CFA injection was greatly increased (fig. 6A), and the relative intensity of CGRP immunoreactivity was significantly increased to 1.24 ± 0.24 ($P < 0.01$; fig. 6B). In contrast, CGRP immunoreactivity in the SDH was not increased even at 24 h after incision (fig. 6A); the relative intensity of CGRP immunoreactivity was 0.98 ± 0.19 (fig. 6B).

Because we used an antibody against both αCGRP and βCGRP in this experiment, there is the possibility that βCGRP expression was increased in the SDH. Therefore, we examined CGRP expression in the SDH in αCGRP knockout mice. CGRP immunoreactivity was below the detection level in naive αCGRP knockout mice at 24 h after CFA injection (fig. 6C), suggesting that αCGRP expression but not βCGRP expression was increased in the SDH after CFA-induced inflammation.



Copyright © by the American Society of Anesthesiologists. Unauthorized reproduction of this article is prohibited.

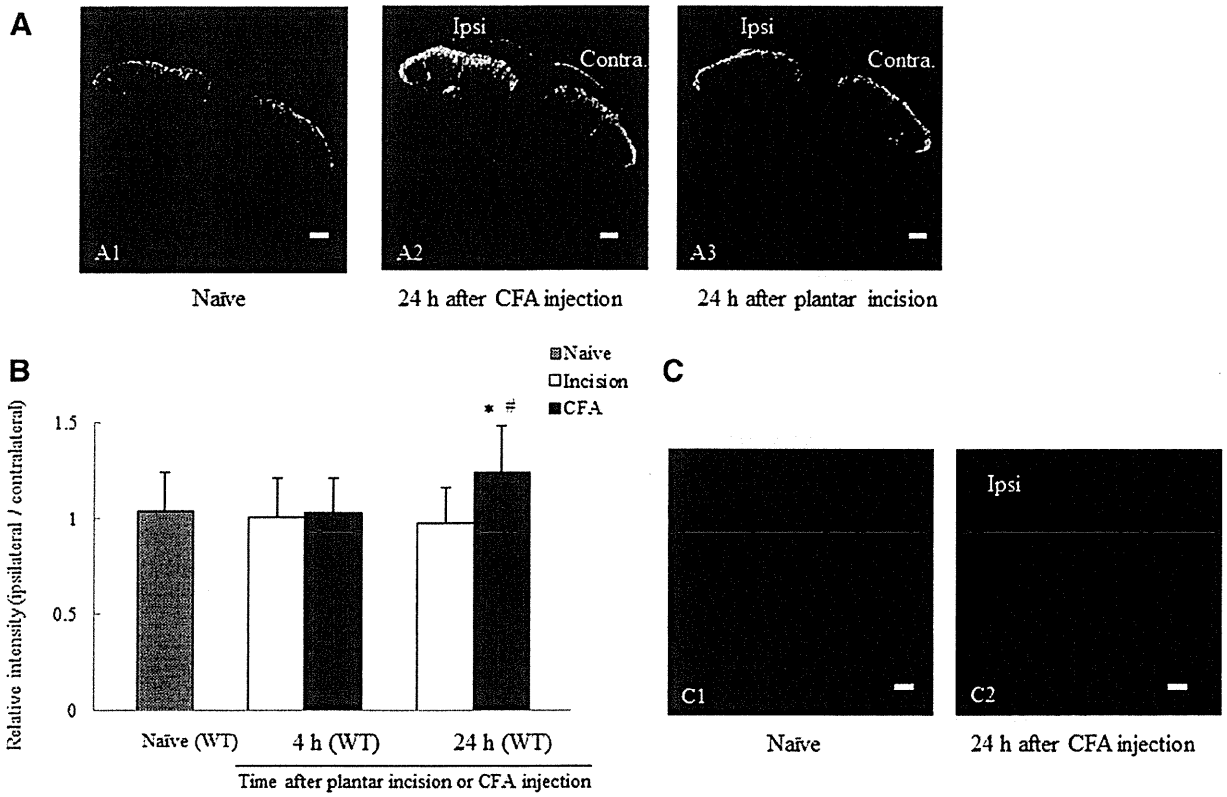


**Fig. 6.** Calcitonin gene–related peptide (CGRP) expression in the superficial dorsal horn (SDH) of the spinal cord after incision and complete Freund's adjuvant (CFA) injection. (*A*) Representative αβCGRP expression in the SDH of the L4 to L5 segments. *A1* showed that in naive wild-type (WT) mice. *A2* showed that in WT mice at 24 h after CFA injection. *A3* showed that in WT mice at 24 h after incision. *Scale bar* = 100 μm. (*B*) Relative intensity of CGRP immunoreactivity after incision and CFA injection. (*C*) Representative αβCGRP expression in the SDH of the L4 to L5 segments. *C1* showed that in naive αCGRP knockout mice. *C2* showed that in αCGRP knockout mice at 24 h after CFA injection. *Scale bar* = 100 μm. n = 4–6 in each group. Intense CGRP immunoreactivity was observed in the SDH of naive mice. CGRP expression was not altered at 4 and 24 h after incision and at 4 h after CFA injection. However, CGRP expression in the SDH on the ipsilateral side was increased at 24 h after CFA injection. CGRP immunoreactivity was below the detection level in naive αCGRP knockout mice and also below the detection level 24 h after CFA injection. Data are expressed as means ± SDs. **P* < 0.01, *versus* 4 h after CFA injection. #*P* < 0.01, *versus* naive. Contralateral (contra.) = paw on the contralateral side to incision or CFA injection; ipsilateral (ipsi.) = paw on the ipsilateral side to incision or CFA injection.

### *c-Fos Expression in the SDH after Plantar Incision and CFA Injection*

Few c-Fos–positive neurons were observed in the SDH in naive mice that did not receive incision or CFA injection (data not shown). The numbers of c-Fos–positive neurons in the SDHs on the ipsilateral side to the incision and CFA injection were significantly increased at 4 h after incision and CFA injection compared with those on the contralateral side ($P < 0.0001$; fig. 7, A and B). There were no significant differences in the number of c-Fos–positive neurons between the incision group and CFA injection group in WT mice. The increased number of c-Fos–positive neurons was maintained at 24 h after CFA injection, whereas the number of c-Fos–positive neurons was greatly decreased at 24 h after incision and was comparable with that on the contralateral side (fig. 7B).

Complete Freund's adjuvant injection significantly increased the number of c-Fos–positive neurons in the SDH on the ipsilateral side to injection in αCGRP knockout mice at 4 and 24 h after CFA injection ($P < 0.01$; fig. 7, A and B). The number of c-Fos–positive neurons in αCGRP knockout mice was comparable with that in WT mice at 4 h after CFA injection. However, the number of c-Fos–positive neurons in αCGRP knockout mice was significantly lower than that in WT mice at 24 h after CFA injection ($P < 0.0001$; fig. 7B).

## Discussion

New findings in this study are as follows: (1) αCGRP is not involved in incision-induced spontaneous pain assessed as GPS, thermal hyperalgesia, or mechanical hyperalgesia, (2) αCGRP plays an important role in inflammation-induced spontaneous pain and thermal hyperalgesia but not in mechanical hyperalgesia, (3) αCGRP is involved in the late



Copyright © by the American Society of Anesthesiologists. Unauthorized reproduction of this article is prohibited.

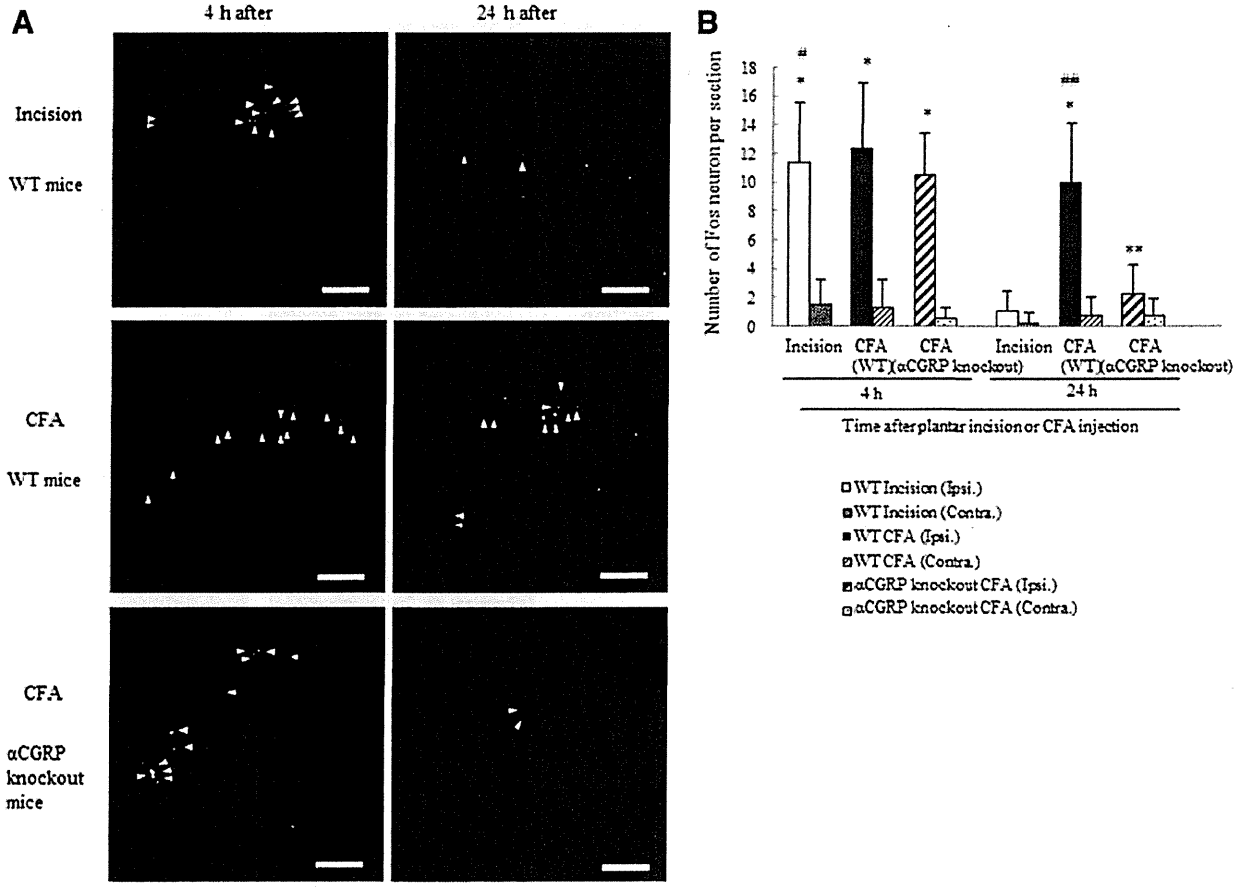


**Fig. 7.** Changes in c-Fos expression in the superficial dorsal horn (SDH) of the spinal cord after incision and complete Freund's adjuvant (CFA) injection. (*A*) Representative c-Fos expression in the SDH of the L4 to L5 segments at 4 and 24 h after incision and CFA injection in wild-type (WT) mice and α-calcitonin gene–related peptide (αCGRP) knockout mice. All *photographs* show the SDH on the ipsilateral side to incision or CFA injection. *Arrowheads* indicate c-Fos–positive neurons, and *red dashed lines* indicate the ventral boarder of the SDH defined by protein kinase Cγ expression. *Scale bar* = 100 μm. (*B*) Numbers of c-Fos–positive neurons in the SDH at 4 and 24 h after incision and CFA injection. n = 4–6 in each group. The number of c-Fos–positive neurons in the SDH of WT mice was significantly increased at 4 h after incision but had returned to the basal level at 24 h after incision. The c-Fos–positive profile in WT mice and αCGRP knockout mice was significantly increased at 4 h after CFA injection, and a significant increase in c-Fos expression was also observed at 24 h after CFA injection in WT mice but not in αCGRP knockout mice. Data are expressed as means ± SDs. **P* < 0.0001, *versus* contralateral side. ***P* < 0.01, *versus* contralateral side. #*P* <0.0001, *versus* 24 h after incision. ##*P* <0.0001, *versus* αCGRP knockout mice 24 h after CFA injection. Contralateral (contra.) = contralateral side to incision or CFA injection; ipsilateral (ipsi.) = ipsilateral side to incision or CFA injection.

phase (24 to 72 h after CFA injection) but not in the early phase (within 6 h after CFA injection) of inflammation-induced pain, and (4) spinal action but not peripheral action of αCGRP is involved in CFA-induced thermal hyperalgesia.

### *Spinal CGRP for Nociception in a Normal Condition*

It has been reported that intrathecal $CGRP_{8-37}$ had antinociceptive effects against nociceptive thermal and mechanical stimuli in a normal condition.[17] However, it has also been shown that intrathecal antiserum against CGRP did not have any analgesic effects on heat and mechanical nociception in a normal condition.[18] An electrophysiological study also showed that spinal application of $CGRP_{8-37}$ had no significant effect on normal synaptic transmission in SDH neurons.[19] Both calcitonin and αCGRP gene–deficient mice showed normal response to noxious heat stimuli.[6] To determine the involvement of αCGRP alone in various pain states, research focusing on depletion of αCGRP alone is necessary. Thus, we have developed mice in which αCGRP alone is depleted.[9] The fact that normal responses to noxious heat and mechanical stimuli were seen in αCGRP knockout mice in this study confirms that αCGRP does not play an important role in pain transmission in a normal condition.

### *Contribution of αCGRP to Postoperative Pain and Inflammatory Pain*

It is likely that GPSs, PWLs to heat stimuli, and MTs to mechanical stimuli are indices of spontaneous pain, thermal hypersensitivity, and mechanical hypersensitivity, respectively. Because guarding behavior is a nonevoked behavior



Copyright © by the American Society of Anesthesiologists. Unauthorized reproduction of this article is prohibited.

and correlates well with spontaneous activity in dorsal horn neurons,[16] it is considered that guarding behavior reflects spontaneous pain.[12] These components of pain consist of postoperative pain after surgery in a clinical setting. In the current study, there were no significant differences in GPSs, PWLs, and MTs between αCGRP knockout mice and WT mice after incision during the observation period. These results suggest that αCGRP is not involved in spontaneous pain, mechanical hyperalgesia, or thermal hyperalgesia in postoperative pain after surgery.

In the current study, GPSs significantly increased and PWLs to heat stimulation and MTs to mechanical stimulation significantly decreased in both αCGRP knockout mice and WT mice up to 6 h after CFA injection (early phase). The increased GPSs and decreased PWLs gradually returned to the basal levels from 24 to 72 h after CFA injection (late phase) in αCGRP knockout mice, whereas the increased GPSs and decreased PWLs remained relatively constant during the late phase in WT mice. There were no significant changes in MTs between αCGRP knockout mice and WT mice during the late phase after CFA injection. These results suggest that αCGRP is involved in spontaneous pain and thermal hyperalgesia seen in the late phase of inflammatory pain. The results based on antihyperalgesic effects of intrathecal but not intraplantar $CGRP_{8-37}$ strongly suggest that the spinal action but not peripheral action of αCGRP is involved in an inflammatory pain state.

### Mechanisms of αCGRP-induced Inflammatory Pain in the Spinal Cord

Because guarding behavior correlates well with spontaneous activity in dorsal horn neurons,[16] it seems that spontaneous noxious input to spinal neurons persisted only for 2 to 6 h (early phase) and 2 to 72 h (early and late phases) after incision and CFA injection, respectively. Indeed, it has been reported that, in contrast to a plantar incision pain model, high spontaneous activity in SDH neurons is still present 48 h after CFA injection,[12] suggesting sustained noxious inputs to spinal neurons after CFA injection but not after incision. The findings that the number of c-Fos–positive neurons in the SDH was significantly increased at 4 and 24 h in WT mice and only at 4 h after CFA injection and incision, respectively, which are similar to results in previous reports,[20,21] correlated well with the changes in guarding behavior in the current study. Thus, behavioral and c-Fos studies indicate that intense noxious stimuli that are sufficient to evoke spontaneous pain persist longer after CFA injection than those after incision.

Complete Freund's adjuvant–induced inflammation up-regulates CGRP in DRG neurons.[22] In our study, up-regulation of CGRP in the SDH was observed in the late phase but not in the early phase of CFA-induced inflammatory pain. However, CGRP was not up-regulated in the SDH in the early phase or in the late phase after incision. Therefore, sustained noxious inputs that are sufficient to evoke long-term spontaneous pain after CFA injection may increase CGRP expression in the SDH. Repetitive stimulation of C-fibers can activate *N*-methyl-D-aspartate receptors in the SDH,[23] resulting in the release of substance P.[24] Many CGRP-containing primary afferents contain substance P and CGRP,[25] and CGRP and substance P are thought to be coreleased by repetitive stimulation of C-fibers.[26] Thus, CGRP would be up-regulated in the late phase but not in the early phase after CFA injection. This may explain why spinal *N*-methyl-D-aspartate receptors are involved in CFA-induced inflammatory pain[27] but not in incisional pain.[28]

It has been reported that CGRP receptors are localized in glutaminergic presynaptic terminals of the SDH[29] and that spinal application of CGRP increases glutamate release evoked by electrical stimulation of the dorsal root.[30] In a spinal cord slice obtained from an inflammation-induced pain model, the CGRP receptor antagonist $CGRP_{8-37}$ reduced the amplitude of monosynaptic excitatory postsynaptic current although application of CGRP did not affect the frequency of miniature excitatory postsynaptic current.[19] These results suggest that CGRP could facilitate excitatory glutaminergic synaptic transmission in the spinal cord by postsynaptic but not presynaptic mechanisms. Taken together with the fact that activation of *N*-methyl-D-aspartate receptors triggers excessive release of CGRP,[23,24] activation of CGRP receptors as well as glutamate receptors, such as α-amino-3-hydroxy-5-methyl-4-isoxazole propionic acid receptors, *N*-methyl-D-aspartate receptors, and metabotropic glutamate receptors, may contribute to the enhancement of nociceptive transmission in presynaptic and postsynaptic terminals in a coordinated manner in an inflammatory pain state but not in a postoperative pain state.

### Involvement of CGRP in Spontaneous Pain and Thermal Hyperalgesia in an Inflammatory Pain State

Previous electrophysiological studies have suggested that many CGRP-expressing DRG neurons respond to noxious heat and mechanical stimuli being classified as polymodal.[31,32] However, it has also been reported that primary afferents with distinct histochemical characteristics such as expression of transient receptor potential cation channel subfamily V member 1 (TRPV1) and MrgprD are selectively involved in thermal or mechanical hyperalgesia.[33] CGRP is expressed in approximately 80% of TRPV1-positive primary afferent neurons[34] but not in MrgprD-positive neurons, and ablation of TRPV1-positive primary afferents has been shown to selectively abolish inflammation-induced thermal hyperalgesia.[33] A recent study using genetic ablation of αCGRP-expressing primary afferents has also shown that αCGRP-expressing sensory neurons contribute to noxious heat perception and inflammation-induced thermal hyperalgesia but not to noxious mechanical perception or mechanical hyperalgesia.[5] These findings suggest that CGRP is involved in thermal hyperalgesia but not in mechanical hyperalgesia. The results of our study also showed that



Copyright © by the American Society of Anesthesiologists. Unauthorized reproduction of this article is prohibited.